Supporting Information

Fe(II)-Catalyzed Ligand-Controlled Dissolution of Iron(hydr)oxides

Jagannath Biswakarma[1,2], Kyounglim Kang[3], Susan C. Borowski[1#], Walter D.C. Schenkeveld[3†], Stephan M. Kraemer[3], Janet G. Hering[1,2,4] and Stephan J. Hug[1]*

[1]Eawag, Swiss Federal Institute of Aquatic Science and Technology, W&T, CH-8600 Dübendorf, Switzerland

[2] Swiss Federal Institute of Technology (ETH) Zurich, IBP, CH-8092 Zürich, Switzerland

[3] University of Vienna, Dept. of Environmental Geosciences, 1090 Vienna, Austria

[4] Swiss Federal Institute of Technology Lausanne (EPFL), ENAC, CH-1015 Lausanne, Switzerland

[*] Corresponding author. E-mail: stephan.hug@eawag.ch

[#] Current address: Randolph-Macon College, Department of Chemistry, 114 College Avenue, Ashland VA. 23005-5505, USA

[†] Current address: Copernicus Institute of Sustainable Development, Faculty of Geosciences, Utrecht University, Princetonlaan 8A, 3584 CB, Utrecht, the Netherlands

Number of pages : 24
Number of tables : 5
Number of figures : 12

Content

Text S1. Synthesis of Lepidocrocite

The method for synthesis of lepidocrocite (Lp) was modified from Schwertmann. [5] Briefly, 60 mM solution of $FeCl_2$ (71.6 g of $FeCl_2.4H_2O$ in 6 L DDI water, with a pH between 3.53 - 3.79) was purged with N_2 for 2 h. NaOH (~15 mL, 1 M) was titrated slowly to the strongly stirred solution to increase the pH to a range of 6.65 - 6.76. When the pH had stabilized, oxygen was bubbled through the solution to initiate the Fe(II) oxidation process. During the synthesis, the solution was continuously and vigorously stirred and temperature was kept at 15^{o}C. The flow of oxygen was adjusted in the range of 360-1200 ml/min, keeping the base addition constant at 6 ml/min. The pH was kept between 6.60 - 6.75 throughout the synthesis with NaOH (731 ml, 1 M). During the synthesis, the color changed from the initial green-yellow to green-blue, black and then to brown-orange. After 2 h, a bright orange suspension was formed. The suspended particles were collected by centrifugation and repeatedly washed by resuspension and centrifugation with DDI water until the electrical conductivity of the suspension had decreased from 2500 µS/cm to 46 µS/cm. Finally, the solid was collected and dried with stream of N_2. Vigorous stirring and slow addition of NaOH to the reaction mixture, in between the center and the walls of the reaction vessel right above the stirrer were essential to avoid formation of goethite and magnetite as byproducts.

Text S2. Lepidocrocite characterization

X-ray Diffraction. The dried samples of lepidocrocite were analyzed by X-ray diffraction analysis (X'Pert powder diffractometer with XCelerator, PANalytical, Almelo, the Netherlands) to determine the phase purity and to estimate the particle size.

ATR-FTIR spectroscopy. A suspension of synthesized lepidocrocite (30 mg/ml) was prepared in DDI H_2O. One µl from the suspension was air dried on the ATR-element prior to record a FTIR spectra on Biorad FTS 755C instrument equipped with a liquid N_2-cooled mercury cadmium telluride (MCT) detector and a nine reflection ATR unit (SensIR Technologies, Danbury, CT).

Transmission Electron Microscopy. Direct imaging of lepidocrocite was taken in the transmission electron microscope (HD2700Cs, Hitachi, Japan) to estimate the particle shapes and dimensions.

Text S3. Details on ATR-FTIR measurements

FTIR spectra (4000-400 cm^{-1}, 2 cm^{-1} resolution, 32 or 64 scans) were recorded on a Biorad FTS 575C instrument equipped with a liquid N_2-cooled mercury cadmium telluride (MCT) detector and a nine reflection diamond ATR unit (SensIR Technologies, Danbury, CT). Absorbance spectra were obtained from single beam background spectra (I_0) and single beam sample spectra (I_S), with the relation absorbance=$\log_{10}(I_0/I_S)$. FTIR spectral analysis were performed with routines written in Matlab.

The following procedure was employed before performing any dissolution experiments. A single-beam spectrum of the blank ATR crystal was measured as the background spectrum for the calculation of absorbance spectra of an initial Lp layer. A thin layer of 40-60 µg Lp was formed on the ATR crystal (diamond, ϕ 4 mm) by spraying 2 µL of a 30 mg/mL Lp suspension with an ultra-sonicator tip (Sonozap ultrasonic atomizer). IR absorbance spectra of the Lp layer were recorded after drying the layer with a gentle stream of N_2. The layer was rinsed several times with a gentle stream of DDI water and subsequently dried, until the absorbance did not decrease due to detachment of loosely adhering particles. Subsequently, a 50 ml polypropylene beaker was mounted onto the ATR unit and the layer was covered with 40 ml aqueous solution of 9.5 mM NaCl (38 ml 10 mM NaCl) and 5 mM MES/MOPS (2 ml 100 mM MES/MOPS stock solution).

Continuous purging of the aqueous solution with high purity N_2 gas (Alpha gas N_2, 99.999% pure, O_2 < 0.1 ppm, H_2O< 0.5 ppm) lead to desorption of adsorbed CO_2 from Lp and served to stir the solution during measurements. O_2 concentrations were optically measured using PreSens Fibox 4 trace oxygen sensor (PreSens precision sensing GmbH, Germany). Oxygen is measured with a luminescent oxygen sensor spot fixed on the inner wall of the reaction cell. Residual oxygen concentrations after 3 h of purging with N_2 were < 10 nM. At this point a new single-beam background spectrum with the Lp-layer in contact with the anoxic background electrolyte was recorded. Subsequently, absorbance spectra were measured continuously, every 43 s or 71 s. Since these absorbance spectra display the differences developing with the addition of EDTA and Fe(II), they are termed difference absorbance (ΔA) spectra.

To measure the adsorption isotherm of EDTA on lepidocrocite at pH 6, 10-200 µM EDTA were added to the deoxygenated aqueous solution (40ml 10 mM NaCl, 5 mM MES)

covering lepidocrocite layer in the ATR unit. FTIR spectra were recorded continuously to follow the characteristic changes (increase/decrease) of absorbance. In an another experiment, 50 µM EDTA was added to lepidocrocite layer at different pH ranges (pH 3-6) to observe the spectral changes of adsorbed EDTA due to (de/)protonation.

Text S4. Actinometry

An actinometer solution (1 ml of 1.2 M $K_2C_2O_4$ and 1 ml of 400 mM $FeCl_3*6H_2O$ diluted to 20 ml with DDI H_2O), was stirred with magnetic stirrer and irradiated with the UV-LED lamp through a mask with a circular opening with 4 mm diameter at a distance of 7.25 cm for 120 s (the same distance of the UV-lamp from the 4 mm diameter ATR-diamond crystal). After irradiation, 300 µL of the actinometer solution was withdrawn and mixed with 150 µL 600 mM acetate buffer and with 600 µL 10 mM phenanthroline and diluted to 3.0 ml with DDI H_2O. A UV-visible absorption spectrum of this mixture in 1 cm quartz cell was then measured at 510 nm and the photon flux calculated as described previously. The determined photon flux was 3.55 x 10^{15} photons/s corresponding to an irradiation of 150 W/m^2.

Text S5. Estimation of photochemically produced Fe(II)

The decrease of the absorbance of Lp during the two irradiation periods was 0.01-0.012 absorbance units, which corresponds to 1.4-1.7% dissolution of the 40-60 µg Lp (initial absorbance of ca. 0.8, see Table S2). Assuming that photo-reductive dissolution is the dominant process during illumination, we thus formed 0.14-0.25 µM Fe(II) calculated over the solution volume of 40 ml. We note that in all ATR-FTIR measurements, EDTA was in excess (40 ml of 50 µM EDTA = 2 µmol) compared to Lp in the layer (40-60 µg = 0.45-0.68 µmol Lp and 21-32 nmol surface sites with 63 m^2 g^{-1} and 5 sites nm^{-2}). EDTA was also in large excess over photoproducts formed. During illumination, we observe mainly photo-reductive dissolution as described in previous studies [1-4, 6] and possibly some additional Fe(II)-catalyzed non-reductive dissolution, while we observe only the latter after illumination stops.

Text S6. Kinetic model

Equilibrium reactions in the model are described as forward and back reactions in the input file of the kinetic program ACUCHEM (see Table S5). This means that all equations with a double arrow consist of two equations in the program code and the corresponding equilibrium constant is the ratio of the forward over back-reaction rate coefficients (k_f/k_b). Since we did not aim to determine the kinetics of complex formation for dissolved or adsorbed complexes, we entered a value of $1 \cdot 10^6$ s^{-1} for the unimolecular back reactions and an adjustable parameter for the forward reaction. This makes all equilibrium reactions fast and not rate determining on the investigated time scale. The rate-determining reactions are either the electron transfer (R7) or the detachment of Fe(III)EDTA from the reduced surface site (R8). By variation of rate coefficients, we found that either R7 or R8 or a combination of both steps could be rate determining. Experimentally, we can only measure the rate of formation of dissolved Fe(III)L and we have currently no technique to measure the kinetics of the ET and detachment separately. Since Fe(II) complexed to EDTA is a strongly reducing species, we assigned a fixed value to $k_{7(ET)}$ that is higher than the value for k_8 and adjusted the rate coefficient k_8 for the detachment of Fe(III)L as the rate determining step. When reactions R7 and R8 are combined into one reaction ($\equiv Fe^{III}\text{-}Fe^{II}\text{-}L \rightarrow \equiv Fe^{II} + Fe^{III}L$), the same value for the combined rate coefficient is obtained as the value for the Fe(II)-catalyzed detachment (k_8) listed in Table 1 ($\log(k_8) = -0.64$). Important parameters in the model are the concentration of active sites for the dissolution reactions (p_1 to p_4). The site concentration for the adsorption of Fe(II), EDTA and Fe(III)EDTA were obtained from adsorption data and fits as shown in Figure S10. They agree with ranges for iron(hydr)oxides reported in the literature. [7, 8] The fitted concentration of active sites determined from dissolution experiments were a factor of 50-75 smaller than for the sites for adsorption. Increasing their concentration could be compensated by decreasing k_{ET}, but only in a narrow range. More than a doubling of this site concentration lead to significantly worse fits. A lower concentration of sites that are active for dissolution has been used in models describing the dissolution of hematite [9] and agrees with the understanding that dissolution proceeds on kink and step sites [10] whose concentrations are smaller than the sum of adsorption sites measured in adsorption experiments.

It is important to point out that the purpose of the model is to show that the suggested reactions can

explain the experimental results and to explore the importance of the listed reactions, not to determine rate coefficients. We currently don't have sufficient data to uniquely determine the listed rate coefficients.

Text S7. Structures and photo-reactivity

The observation that the photolysis of adsorbed EDTA starts with the onset of UV-irradiation (Fig. 4) is an indication for inner-sphere complexation of EDTA with Fe(III) at the surface. Un-complexed EDTA is not photo-reactive and the yield of OH-radicals by UV-illumination of Fe(III)hydroxides is low [11] The EDTA must be bound as an inner-sphere complex with a metal to ligand charge transfer (MLCT) absorption band that allows rapid light-induced charge transfer from a bound ligand carboxylate group to a surface Fe(III) site. The photoproduct of EDTA, ED3A [6] with a lower IR-absorbance (due to fewer carbxolyate groups) is partly replaced by excess EDTA from solution in a steady state exchange during UV-illumination and completely after the illumination stops. The continuous formation of Fe(II) on the surface ligand during photo-induced charge transfer lead to both photodissolution and Fe(II)-catalyzed ligand-promoted dissolution during illumination, under both oxic and anoxic conditions. After illumination the Fe(II)-catalyzed dissolution continued under anoxic conditions, but not under oxic conditions. In experiments with phenanthroline (not shown) the same behavior was observed as under oxic conditions. These observations show that Fe(II) formed by UV-irradiation is not protected from oxidation by O_2 and that it can easily be desorbed or complexed by phenanthroline. Added and photo-produced Fe(II) appear to have the same effect on the dissolution of Lp.

Table S1. List of chemicals used in the current study

Chemical name	Chemical formula	Supplier	Purity	Stock solution (mM)
Sodium chloride	NaCl	Merck	>99%	10
Fe(II)	$FeCl_2. 4H_2O$	Sigma-Aldrich	>99%	10
Fe(III)	$FeCl_3. 6H_2O$	Sigma-Aldrich	>98%	10
MES (2-morpholino-ethanesulfonic acid monohydrate)	$C_6H_{13}NO_4S. H_2O$	Sigma-Aldrich	>99%	100
MOPS (3-(N-) morpholino propanesulfonic acid)	$C_7H_{15}NO_4S$	Sigma-Aldrich	>99%	100
EDTA (Ethylenediamine tetra acetic disodium dihydate)	$C_{10}H_{14}N_2Na_2O_8. 2H_2O$	Merck	>99%	100
Phenanthroline	$C_{12}H_8N_2. H_2O$	Fluka	>99%	10
Iron-10,000 µg/ml		J.T Baker	For ICPMS standard	

Table S2. Initial IR absorbances of Lp at 1021 cm^{-1}, before conducting Fe(II) added Lp dissolution study. Experiments were conducted in duplicates. Each experiment is listed below as n_1 and n_2.

(To record the initial absorbance, a thin layer of 40-60 µg Lp was formed on the ATR element (diamond, ϕ 4 mm) by spraying 2 µL of a 30 mg/mL Lp suspension with an ultra-sonicator tip and drying with a gentle stream of N_2 (The background single-beam spectrum for the calculation of the absorbance spectrum was the spectrum of the blank ATR-crystal)).

Added Fe(II) concentration (µM)	Lp IR-Absorbance	
	n_1	n_2
0	0.80	0.87
0.2	0.84	0.86
0.5	0.88	0.60
1	0.80	0.87
2	0.87	0.72
4	0.75	0.87
6	0.78	0.87
10	0.90	1.05

Table S3. Dissolution rates of lepidocrocite in presence of 50 µM EDTA with varied added Fe(II) concentrations. All experiments were conducted at pH 6 under anoxic condition and in duplicates. Each experiment is listed below as n_1 and n_2.

Added [Fe(II)] (µM)	Lp dissolution rate (% h^{-1})			Catalytic Effect (CE)*
	ATR-FTIR measurements[a] (Fig.3)			
	n_1	n_2	Average (n_1:n_2)	
0.0	0.17	0.14	0.16	1
0.2	0.86	1.28	1.07	7
0.5	2.10	2.47	2.29	14
1.0	2.97	3.19	3.08	19
2.0	3.12	3.99	3.56	22
4.0	3.90	4.35	4.13	26
6.0	4.41	3.93	4.17	26
10.0	5.50	4.43	4.97	31
Batch measurements[b] (Fig. 5)			n_1	CE
Only in presence of EDTA			0.16	1
1.2 µM ^{57}Fe(II) was added 1800 s after EDTA addition			2.14	13
1.2 µM ^{57}Fe(II) was added 1800 s before EDTA addition[c]			2.40	15

*****CE = $R_{diss,L,Fe(II)}$/ $R_{diss,L}$

$R_{diss,L,Fe(II)}$ is the rate of Fe(II)-catalyzed dissolution in presence of a ligand and Fe(II).

$R_{diss,L}$ is the rate of dissolution in presence of a ligand alone.

With this definition, the CE is 1 if there is no catalytic effect.

[a] In ATR-FTIR measurements, Lp concentration was 10-17 µM. 50 µM EDTA was added 1800 s before Fe(II) addition. Slopes for determining rates were calculated within 3000-5000 s (EDTA addition considered as t=0).

[b] In isotope exchange and dissolution batch studies, Lp concentration was 1125 µM. Slopes were calculated within 2400-4200 s to determine the dissolution rates.

[c] In ATR-FTIR measurements, when 1 µM Fe(II) was added 1800 s before EDTA addition, the rate of Lp dissolution was calculated 2.20 % h^{-1} (Fig. S4).

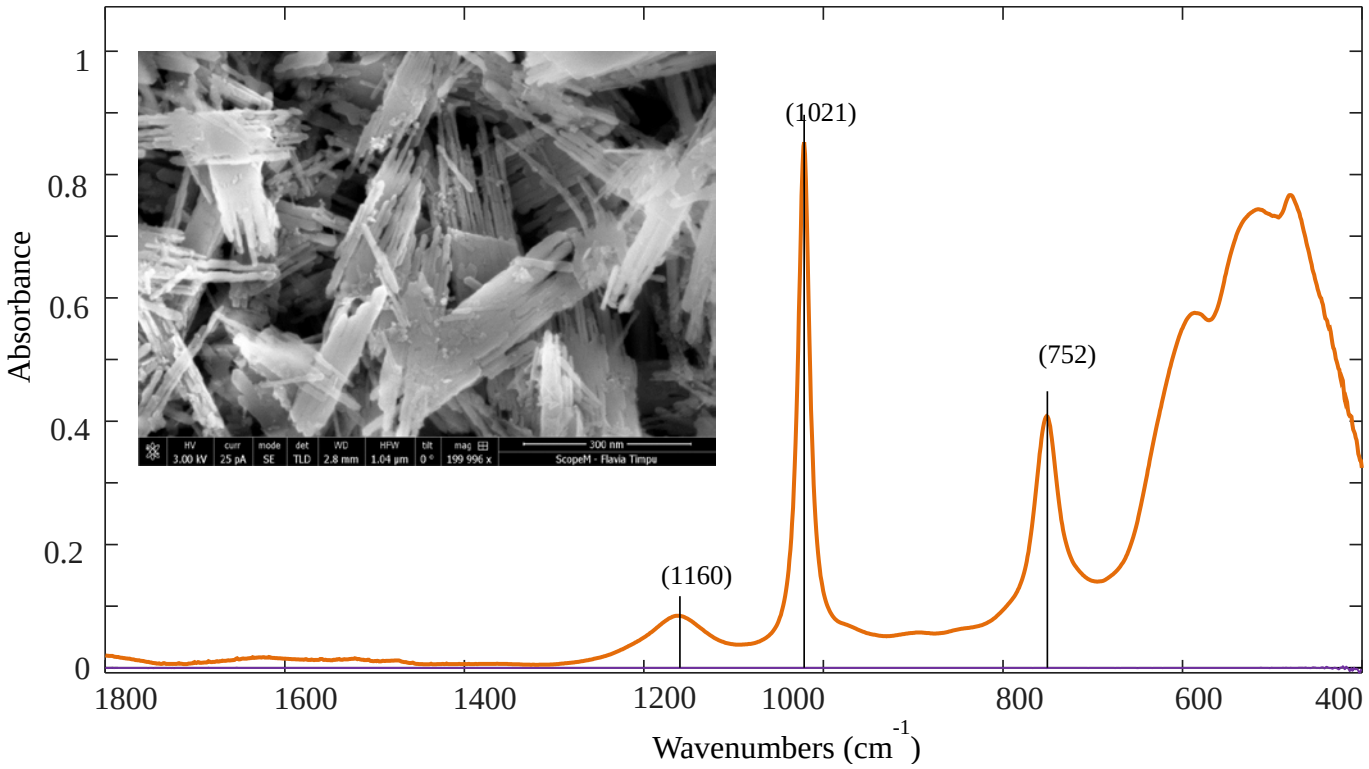

Figure S1. ATR-FTIR absorbance spectrum of synthesized Lp (lepidocrocite). A thin layer of 40-60 µg Lp was formed on the ATR element (diamond, ϕ 4 mm) by spraying 2 µL of a 30 mg/mL Lp suspension with an ultra-sonicator tip and drying with a gentle stream of N_2 (The background single-beam spectrum for the calculation of the absorbance spectrum was the spectrum of the blank ATR-crystal).

The characteristic peaks at 1160 and 1021 cm^{-1} correspond to in-plane bending (δ-OH) and 752 cm^{-1} to outer-plane banding (δ-OH) of Lp structure.

The inset is the transmission electron microscope image of Lp structure.

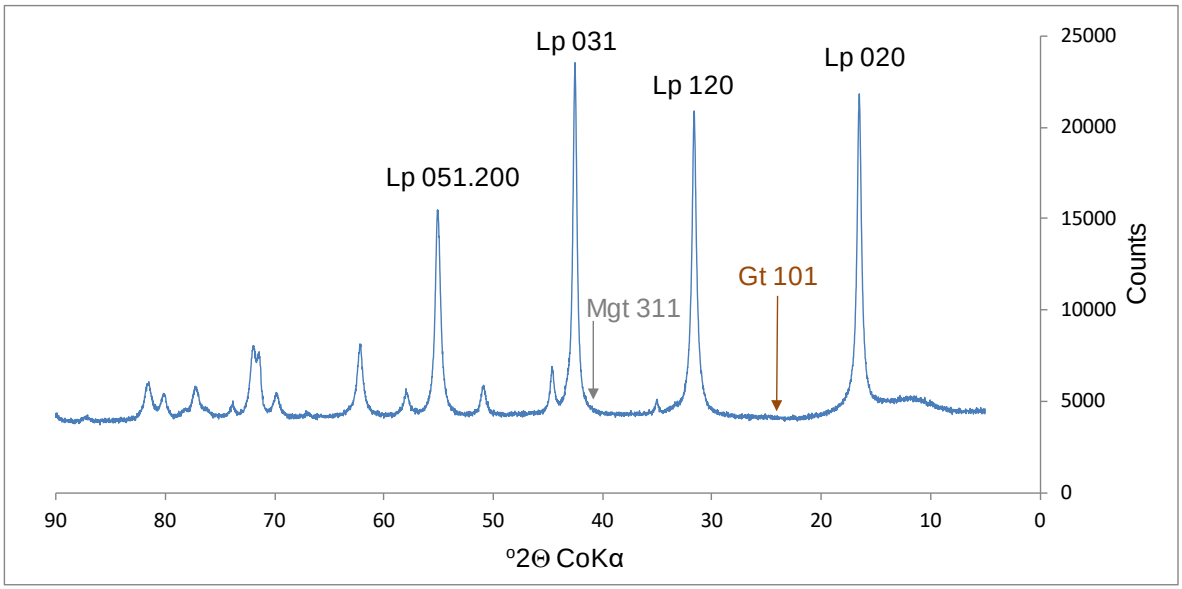

Figure S2. XRD powder diffractogram of the synthesized Lp (lepidocrocite) measured on X'Pert powder diffractometer with XCelerator, PANalytical, Almelo, the Netherlands). The diffractogram is in excellent agreement with lepidocrocite spectra reported by Cornell and Schwertmann.[5] Lines of magnetite (Mgt) and of goethite (Gt), which are common impurities in synthesized Lp, are not detectable.

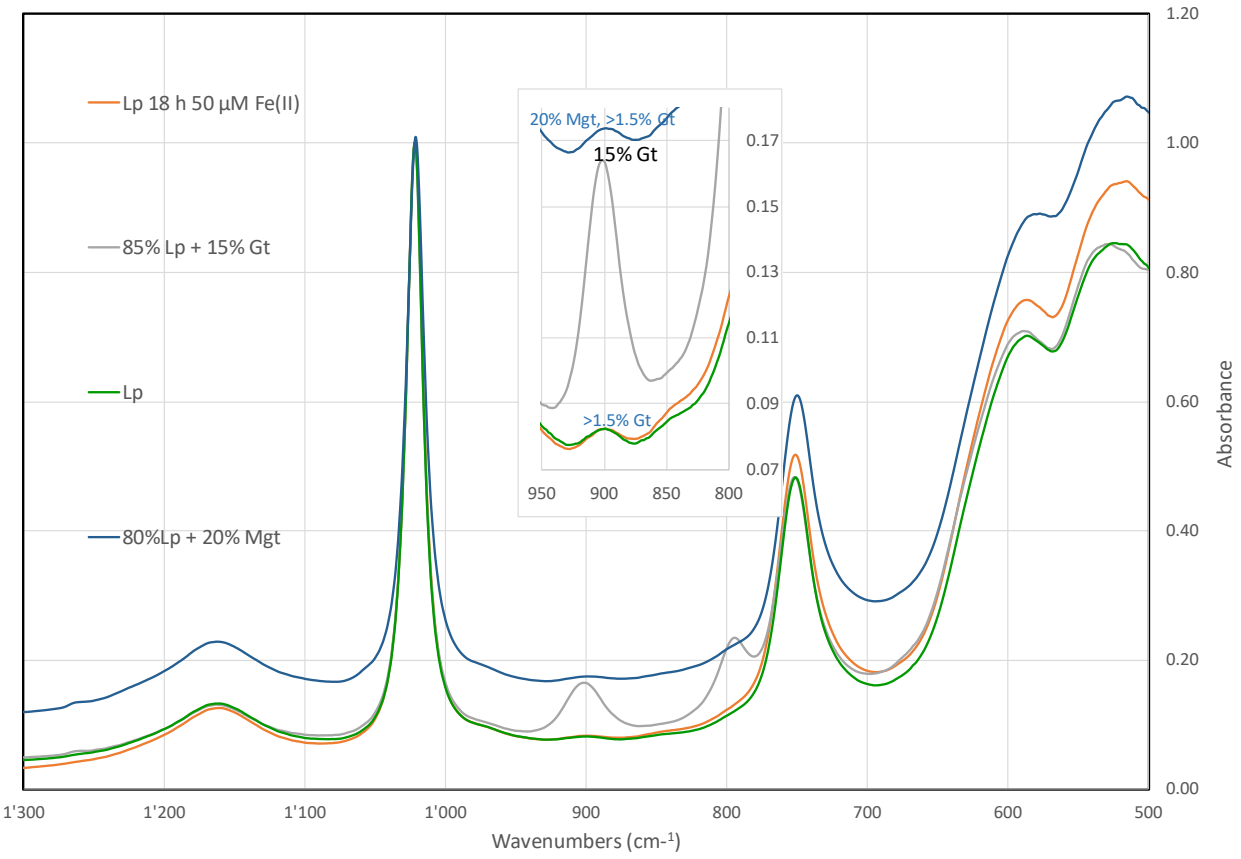

Figure S3. ATR-FTIR spectra of dried layers of various samples: Lp: freshly made Lp- suspension, Lp 18 h 50 µM Fe(II): Lp suspension with 10 mg Lp /100 ml exposed to 50 µM Fe(II) at pH 8.0 under anoxic conditions for 18h, 85% Lp + 15 % Gt: Lp and goethite (Gt) suspensions were mixed to achieve the indicated mass % mixture. Goethite was synthesized as described in Kang et al. [12]. 80% Lp + 20% magnetite (Mgt): suspensions mixed to achieve the % in weight. Magnetite was from MK-nano, Fe_3O_4, 99% Pure, APS: 25 nm (https://www.mknano.com/Nanoparticles/Single-Element-Oxides).

Samples of 2 ml suspensions were filtered through 0.2 um nylon filters and washed with 2 ml nanopure H_2O. The filtrate was resuspended in 2-5 µl H_2O and transferred onto the ATR-diamond disk and dried in a stream of N_2 before absorbance spectra were measured. Traces of goethite in lepidocrocite and changes in goethite fractions can be detected with a sensitivity of better than 1%. Formation of magnetite can be detected by a broad increase of absorbance.

In our experiments with 1-10 µM added Fe(II), we did not detect formation of goethite or magnetite on the time scale of our experiments. Our synthesized Lp contained a fraction of < 1.5% Gt impurity (which was detectable with FTIR, but not in the XRD diffractogram). This fraction did not change during our experiments. We did not observe formation of Gt or Mgt during our experiments with 0.2-10 µM Fe(II).

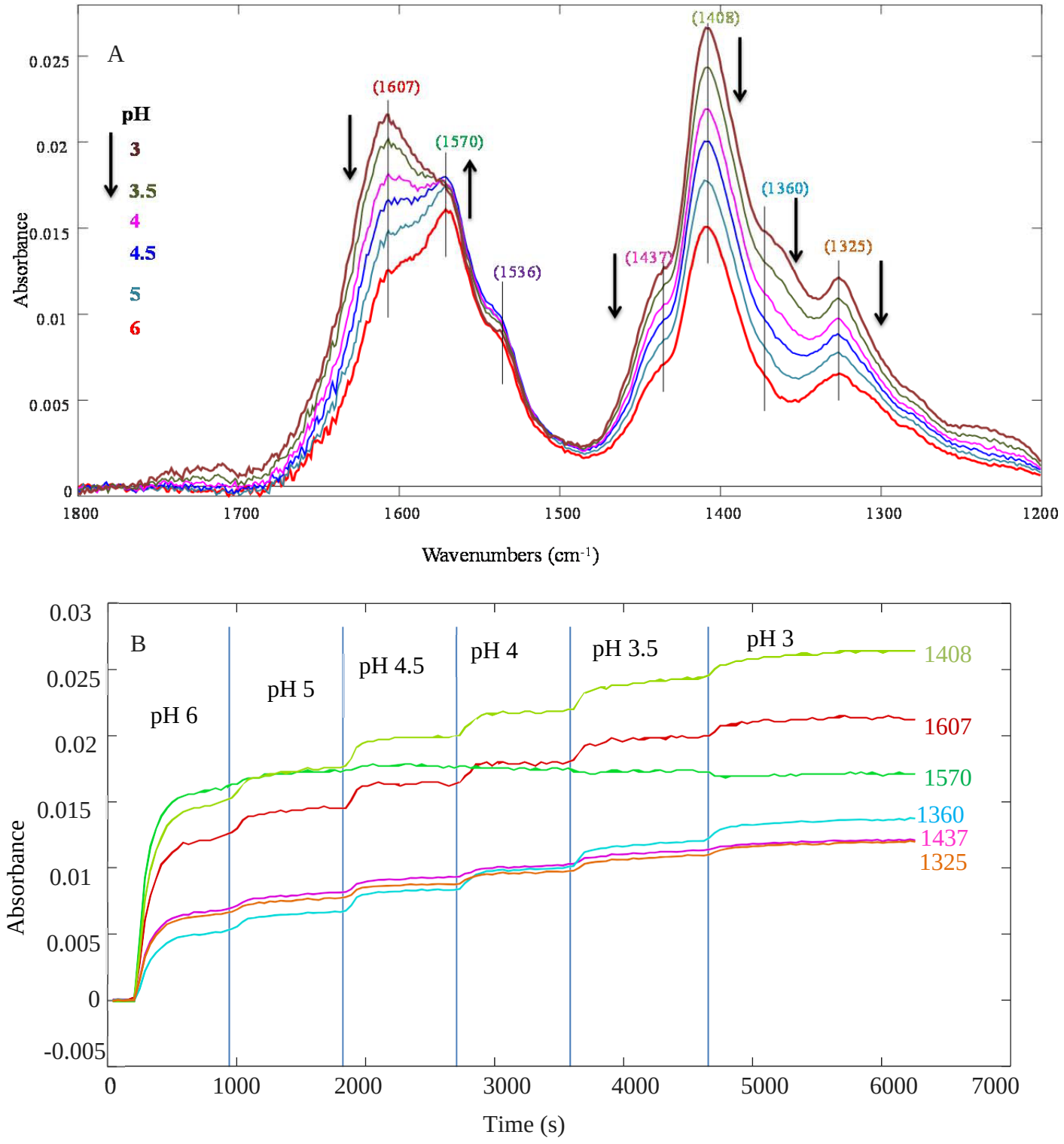

Figure S4. ATR-FTIR difference (background subtracted) (A) absorbance spectra recorded during EDTA adsorption onto lepidocrocite (Lp) and (B) kinetics at pH 3-6 under anoxic condition. The spectrum of Lp in contact with 40 ml aqueous solution (0.01 M NaCl and 0.005 M MES) after purging with high purity N_2 for 3-4 h, before addition of 50 µM EDTA, was defined as background. The pH adjustments were done with minute addition of 0.1 M HCl or NaOH only when EDTA adsorption reached equilibrium at each pH.

The amplitude of EDTA absorbance (recorded as indicated wavenumbers) decreases with increasing pH (pH 3-6), except at 1570 cm^{-1}. The spectral changes occurred upon pH variations indicate that the type of surface complex formed at the surface of lepidocrocite is pH dependent.

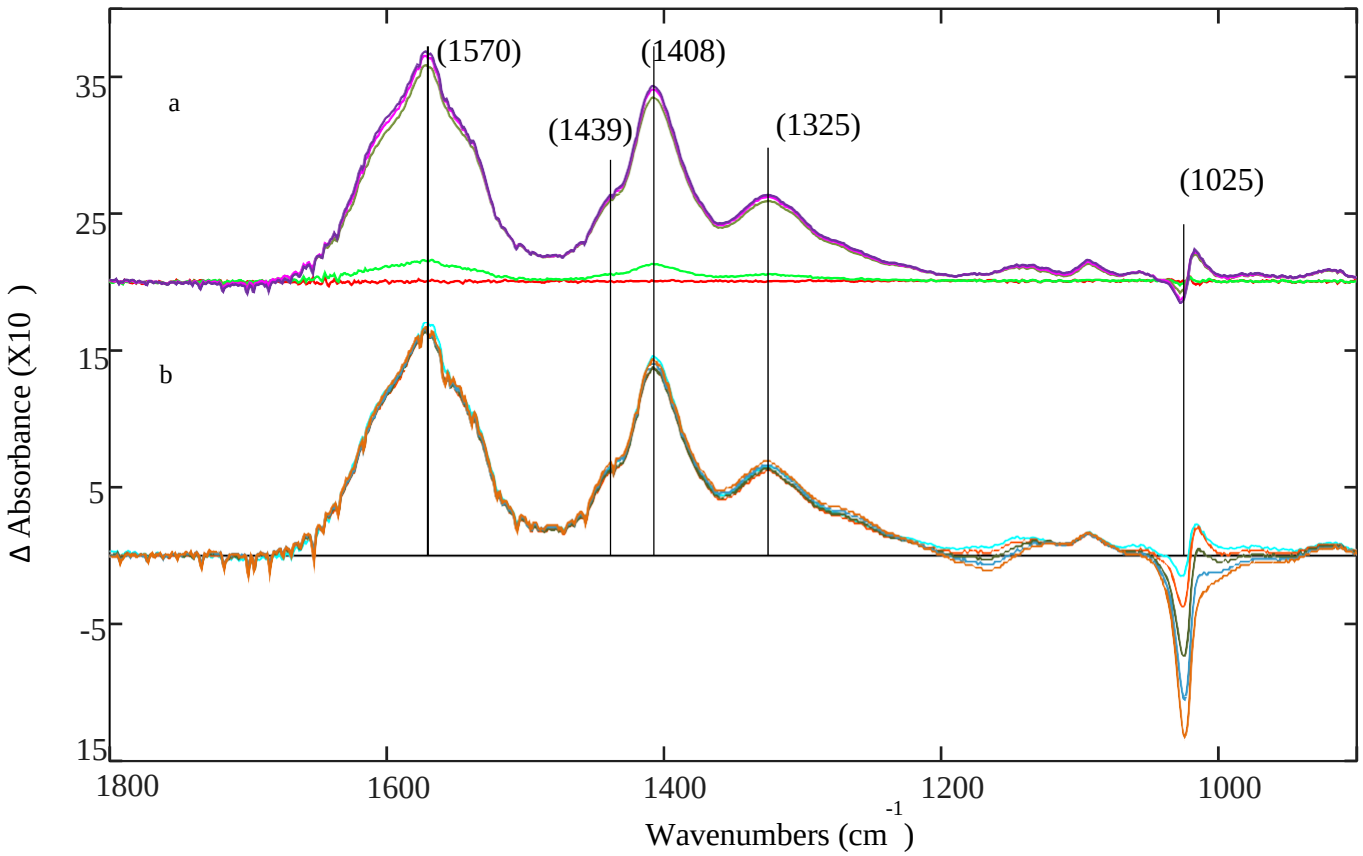

Figure S5. ATR-FTIR difference absorbance spectra (background subtracted), at pH 7, recorded during a) EDTA adsorption (offset by 20 units), upon addition of 50 µM EDTA to a layer of 50-60 µg lepidocrocite (Lp) in contact with 40 ml aqueous solution, and b) dissolution of Lp after addition of 10 µM Fe(II) in presence of 50 µM EDTA (no offset). The spectrum of Lp in contact with aqueous solution (0.01 M NaCl and 0.005 M MOPS) after purging with high purity N_2 for 3-4 h, before addition of EDTA, was defined as background. Spectra were recorded continuously every 71 s. Averages of every 6-10 continuous spectra are shown for clarity.

The group of spectra in a) shows two characteristic peaks of adsorbed EDTA at 1570 cm^{-1} and 1408 cm^{-1} upon addition of EDTA and very minor dissolution of Lp at 1025 cm^{-1}. The group of spectra in b) shows the strongly accelerated dissolution of Lp at 1025 cm^{-1} after addition of 10 µM Fe(II) ($t_{Fe(II)\ addition}$=3000 s, when $t_{EDTA\ addition}$= 800-900 s).

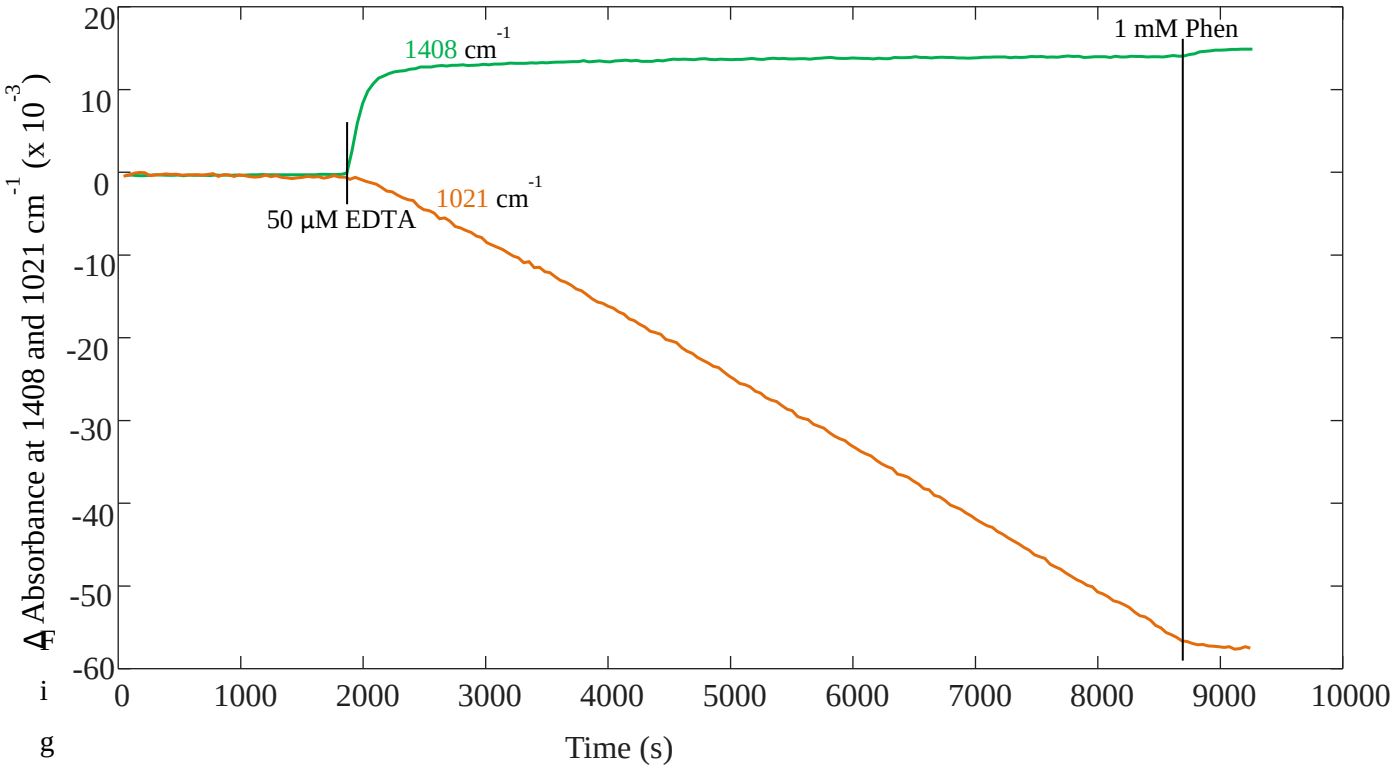

Figure S6. Kinetics of EDTA adsorption (monitored at 1408 cm^{-1}) and lepidocrocite (Lp) dissolution (monitored at 1021 cm^{-1}) with ATR-FTIR at pH 6 under anoxic conditions. 50 µM EDTA was added 1800 s after 1 µM Fe(II) was added, followed by addition of 1 mM phenanthroline (Phen) after 8600 s. The data are shown without normalizing to initial Lp absorbance (0.7-0.9 at 1021 cm^{-1}).

Fe(II) addition didn't cause any significant changes to Lp in absence of EDTA. EDTA addition at 1800 s immediately caused the accelerated dissolution of Lp. EDTA adsorbed fast and reached equilibrium in < 200 s. Phen addition stopped the accelerated dissolution of Lp.

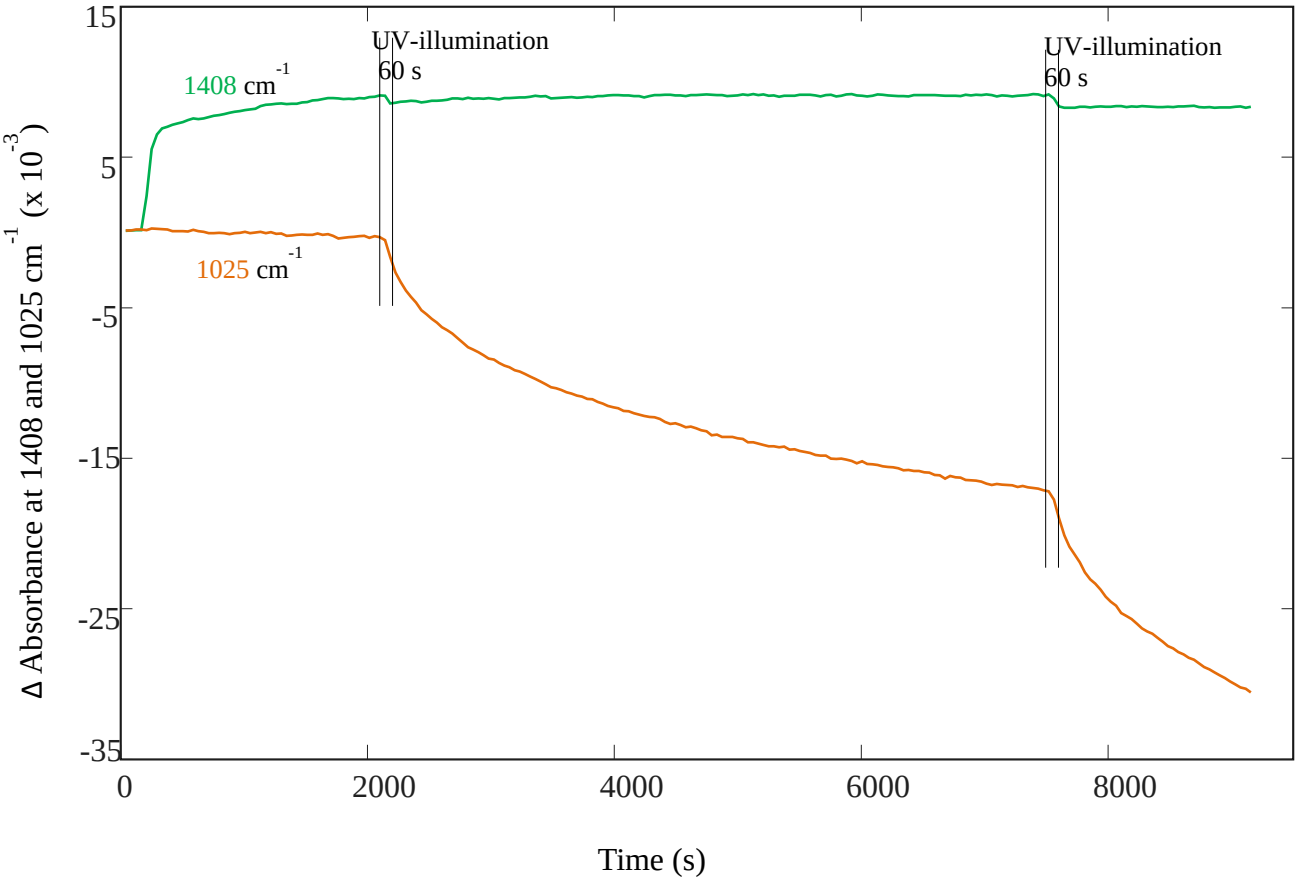

Figure S7. Kinetics of EDTA adsorption (monitored at 1408 cm^{-1}) and dissolution of lepidocrocite (Lp) (monitored at 1025 cm^{-1}) at pH 7 (*I*=0.01 M) under anoxic conditions during photochemical experiments.

EDTA (50 µM) was added at 180-220 s. During UV-illumination (for 60 s, 2 times) with a 365 nm UV-LED lamp, adsorbed EDTA is photolyzed at the surface. After irradiation, photo-transformed EDTA is replaced by EDTA from solution. Lp dissolution was strongly accelerated by UV-illumination. After irradiation stops under anoxic condition, Lp dissolution continued.

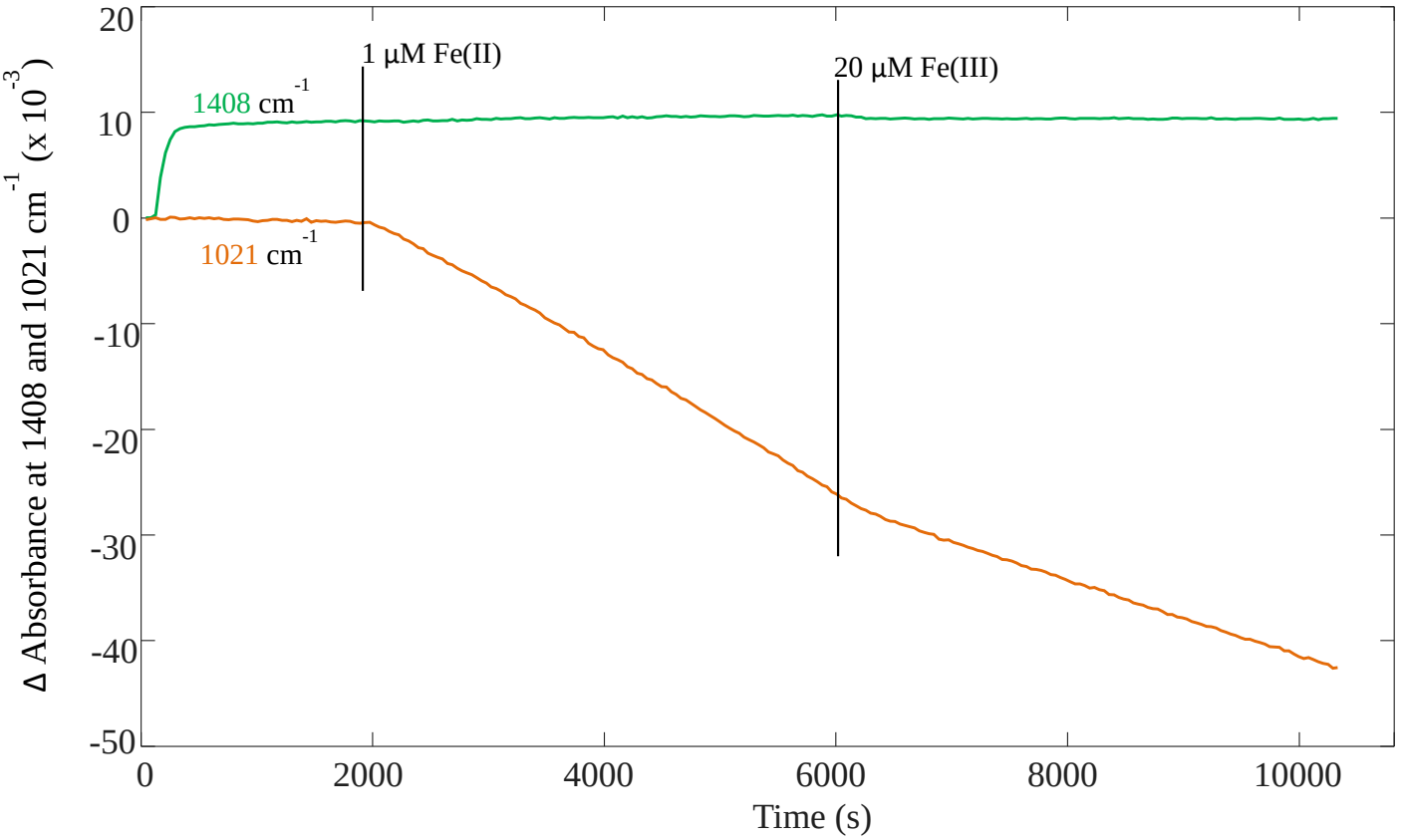

Figure S8. Kinetics of EDTA adsorption (monitored at 1408 cm^{-1}) and lepidocrocite (Lp) dissolution (monitored at 1021 cm^{-1}) with ATR-FTIR at pH 6 under anoxic conditions. 50 µM EDTA was added (at t=180-200 s) after purging the aqueous solution covering the Lp layer with N_2 for at least 3-4 h, followed by addition of 1 µM Fe(II) after 1800 s and addition of 20 µM Fe(III) after 6000 s. The data are shown without normalizing to initial Lp absorbance (0.7-0.9 at 1021 cm^{-1}).

EDTA adsorbed fast and reached equilibrium in < 200 s. 1 µM Fe(II) addition lead to accelerated dissolution of Lp. Addition of 20 µM Fe(III) slowed down the accelerated dissolution.

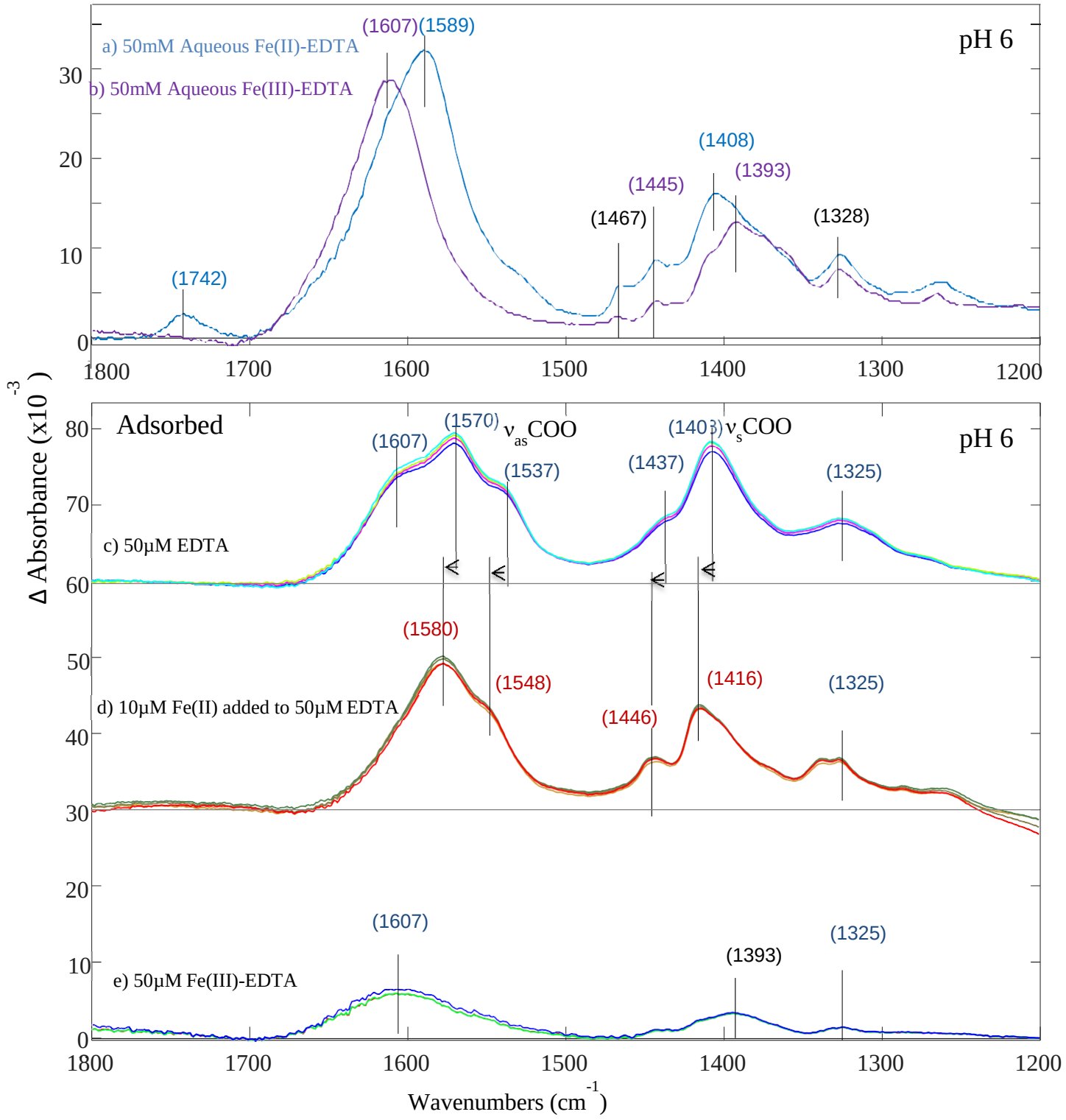

Figure S9. ATR-FTIR spectra of aqueous 1:1 complex of 50 mM (a) Fe(II)-EDTA and (b) Fe(III)-EDTA in top panel. In bottom panel, ATR-FTIR difference absorbance spectra recorded during (c) EDTA adsorption (offset by 60 units), upon addition of 50 µM EDTA to a layer of 50-60 µg lepidocrocite (Lp) in contact with 40 ml aqueous solution, (d) EDTA adsorption, upon addition of 10 µM Fe(II) after 1800 sec of 50 µM EDTA was added (offset by 30 units), and (e) adsorption of 1:1 aqueous complex of 50µM Fe(III)-EDTA onto lepidocrocite (no offset). All the measurements were conducted at pH 6 under anoxic condition.

Table S4. Comparison of experimental IR frequencies

Assignments	Aqueous EDTA	Aqueous Fe(II)-EDTA	Aqueous Fe(III)-EDTA	Adsorbed EDTA	Addition of 10 μM Fe(II) to Lp in presence of EDTA	Adsorbed Fe(III)-EDTA
		1742				
ν_{as} C-O *	1613		1607	1607		1607
ν_{as} C-O *	1575	1589		1570	1580	
ν_{s} C-O *	1456	1467	1467	1537	1548	
ν_{s} C-O *	1433	1445	1445	1437	1446	
ν_{s} C-O *	1402	1408	1393	1408	1416	1393
n.a.	1357					
n.a.	1322	1328	1328	1325	1325	1325

* ν_{as}C-O and ν_{s}C-O are simplified labels. They describe the asymmetric and symmetric carboxylate C-O stretching vibrations that contribute most to the intensity in these spectral regions. The vibrational modes giving rise to the several peaks and shoulders that also contain various contributions of νC-C, δN-H, δCH2 and other vibrations.

n.a. = non-assigned.

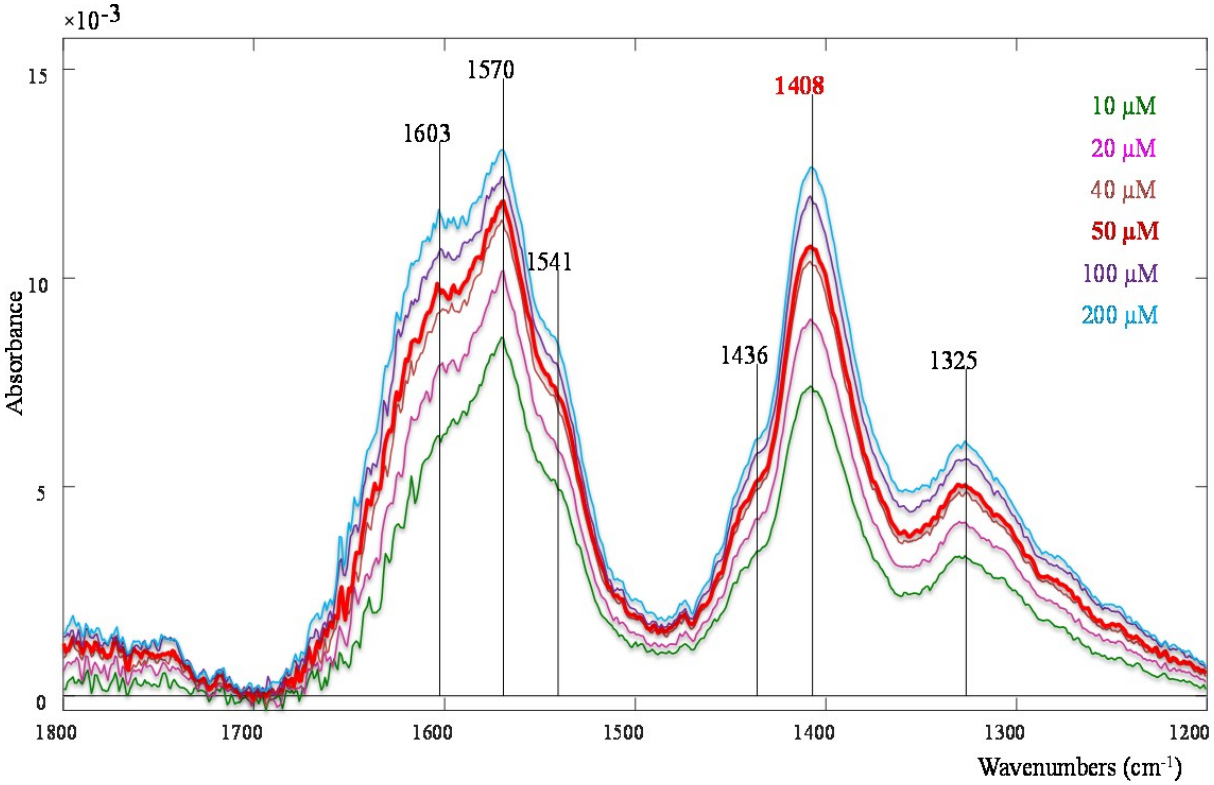

Figure S10. ATR-FTIR difference (background subtracted) absorbance spectra recorded during EDTA (10-200 µM) adsorption onto a layer of 50-60 µg lepidocrocite (Lp) in contact with 40 ml aqueous solution at pH 6 under anoxic condition. The spectrum of Lp in contact with aqueous solution (0.01 M NaCl and 0.005 M MES) after purging with high purity N_2 for 3-4 h, before addition of EDTA, was defined as background. The spectra shown here are the spectra of EDTA when it reached adsorption equilibrium at each concentration.

The spectra show characteristic absorbance of EDTA onto Lp in the range of 1700-1200 cm^{-1}. The two characteristic peaks of adsorbed EDTA at 1570 cm^{-1} and 1408 cm^{-1} correspond to asymmetric and symmetric vibrations of carboxylic group, respectively. The spectra show that increasing concentrations (10-200 µM) of aqueous EDTA do not cause significant spectral changes of adsorbed EDTA, except a small increase of the shoulder at 1603 cm^{-1} (which might indicate a slightly higher contribution of protonated surface complex, see Fig. S2), indicating that the type of surface complex formed at the surface of Lp at pH 6 is largely independent of EDTA concentration.

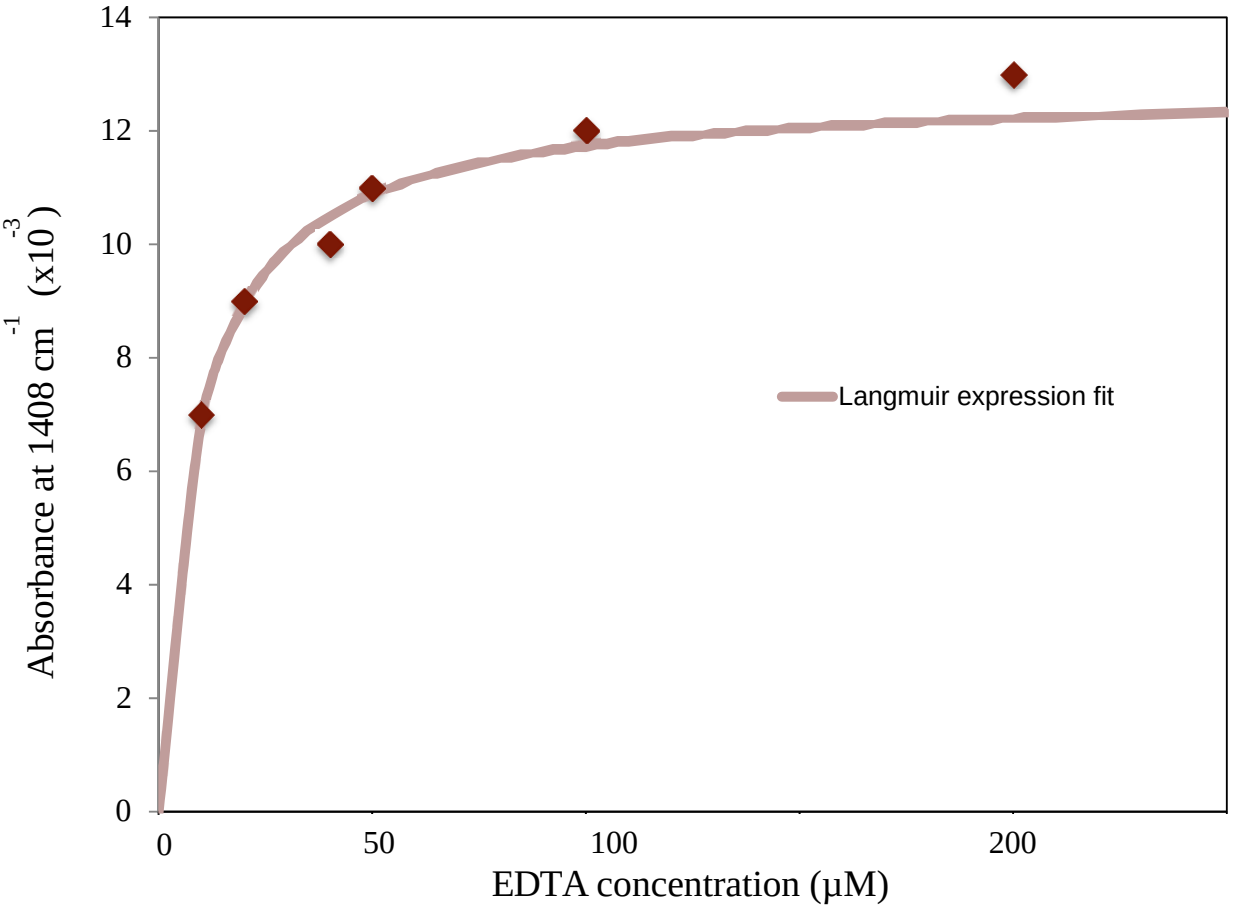

Figure S11. The maximum (absorbance) of EDTA adsorption monitored at 1408 cm^{-1} on lepidocrocite (Lp), with ATR-FTIR at pH 6, plotted as a function of added EDTA concentrations. 10-200 µM EDTA were added after purging the aqueous solution (10 mM NaCl and 5 mM MES) covering the Lp layer (60 µg) with N_2 for at least 3-4 h. The absorbance at 1408 cm^{-1} was fitted with a Langmuir type model (line) to estimate the equilibrium constant for the adsorption of EDTA (see kinetic model). Note that added and equilibrium EDTA concentrations are to within 1% the same in these experiments with only 60 µg Lp and 40 ml aqueous solution (e.g. 6.3 nmol surface sites with 1site/nm^2 versus 800 nmol EDTA in solution with 20 µM EDTA). The surface was considered saturated at $[EDTA]_{aq}$ =200 µM. With [FeOOH] = 10µM in the FTIR experiments and a surface site of concentration of 0.79 sites/nm^2 determined by batch experiments gives 0.072 µM for $[EDTA]_{ads}$ at saturation. A saturated surface concentration of 0.79 sites/nm^2 was similar to 1.12 site/nm^2 obtained by Nowack et al.[8]

Table S5. Kinetic model: input-file for ACUCHEM [a]

```
; INPUT file for ACUCHEM (AC99.EXE)
; Question marks are replaced by adjustable numerical values (fitting parameter or initial conc.)
;
input
0010
;
R1f,    Fe2 + L = Fe2L,              2.17e+16 ; 1     Dissolved Fe2L complex formation [b]
R1b,    Fe2L = Fe2 + L,              1e6
;
R2f,    (SFe3) + L = (SFe3)L,        ?        ;  2    Adsorption of ligand
R2b,    (SFe3)L  = (SFe3)+L,         1e6
;
R3f,    (SFe3) + Fe2 = (SFe3)Fe2,    ?        ;  3    Adsorption of Fe2
R3b,    (SFe3)Fe2 =  (SFe3) + Fe2,   1e6
;
R4f,    (SFe3)Fe2 + L = (SFe3)Fe2L,  ?        ; 4     Adsorption of L on adsorbed Fe2
R4b,    (SFe3)Fe2L = (SFe3)Fe2 + L,  1e6
;
R5f,    (SFe3) + Fe2L = (SFe3)Fe2L,  ?        ; 5     Adsorption of Fe2L
R5b,    (SFe3)Fe2L = (SFe3) + Fe2L,  1e6
;
R6f,    (SFe3) + Fe3L = (SFe3)Fe3L,  ?        ; 6     Competing adsorption of Fe3L
R6b,    (SFe3)Fe3L = (SFe3) + Fe3L,  1e6
;
R7f,    (SFe3)Fe2L = (SFe2)Fe3L,     10       ; 7     Electron transfer
R8f,    (SFe2)Fe3L = (SFe2) + Fe3L,  ?        ; 8     Detachment of Fe3L (rate-determining)
R9f,    (SFe2) + bulk = (SFe3)Fe2,   1e6      ; 9     Formation of new surface site (non-rate determining)
;
R10f,   (SFe3)L  = (S) + Fe3L,       ?        ; 10    Detachment of Fe3L
R11f,   (S) + bulk = (SFe3),         1e6      ; 11    Formation of new surface site
end
;                                    Initial concentrations
(SFe3), ?                            ; 8
 Fe2, ?                              ; 9
L, ?                                 ; 10
bulk,?                               ; 11
Fe3L,?                               ; 12
end
0.0001
 ?                                   ; 13    longest time-point (of 50) in the model in seconds
end
&                                    Additional information for output which is not used by AC99.EXE
9
Fe3L
Fe2L
L
Fe2
(SFe2)Fe3L
(SFe3)L
bulk
(SFe3)Fe2
(SFe3)Fe3L
```

(a) W. Braun, J.T. Herron, D.K. Kahaner, Acuchem: a computer program for modeling complex chemical reaction systems, Int. J. Chem. Kinet. 20 (1988) 51–62.

(b) The conditional equilibrium constant for the complex formation of EDTA with Fe(II) at pH 6.0 in 9.5 mM NaCl was calculated with Visual Minteq (https://vminteq.lwr.kth.se/). With 50 µM EDTA and 1-10 µM dissolved Fe(II), 99.86% of Fe(II) is present as $Fe^{II}EDTA^{2-}$, and only $5 \cdot 10^{-12}$ M is present as non-complexed Fe^{2+}. Towards the end of Lp-dissolution with 50 µM EDTA with 1-2 µM dissolved Fe(II) and 45 µM dissolved Fe(III), 99.86% of dissolved Fe(II) is still present as $Fe^{II}(EDTA)^{2-}$ and Fe(III) is to 97.96% present as $Fe^{III}(EDTA)^{-}$ and to 2.03% as $Fe^{III}(OH)(EDTA)^{2-}$.

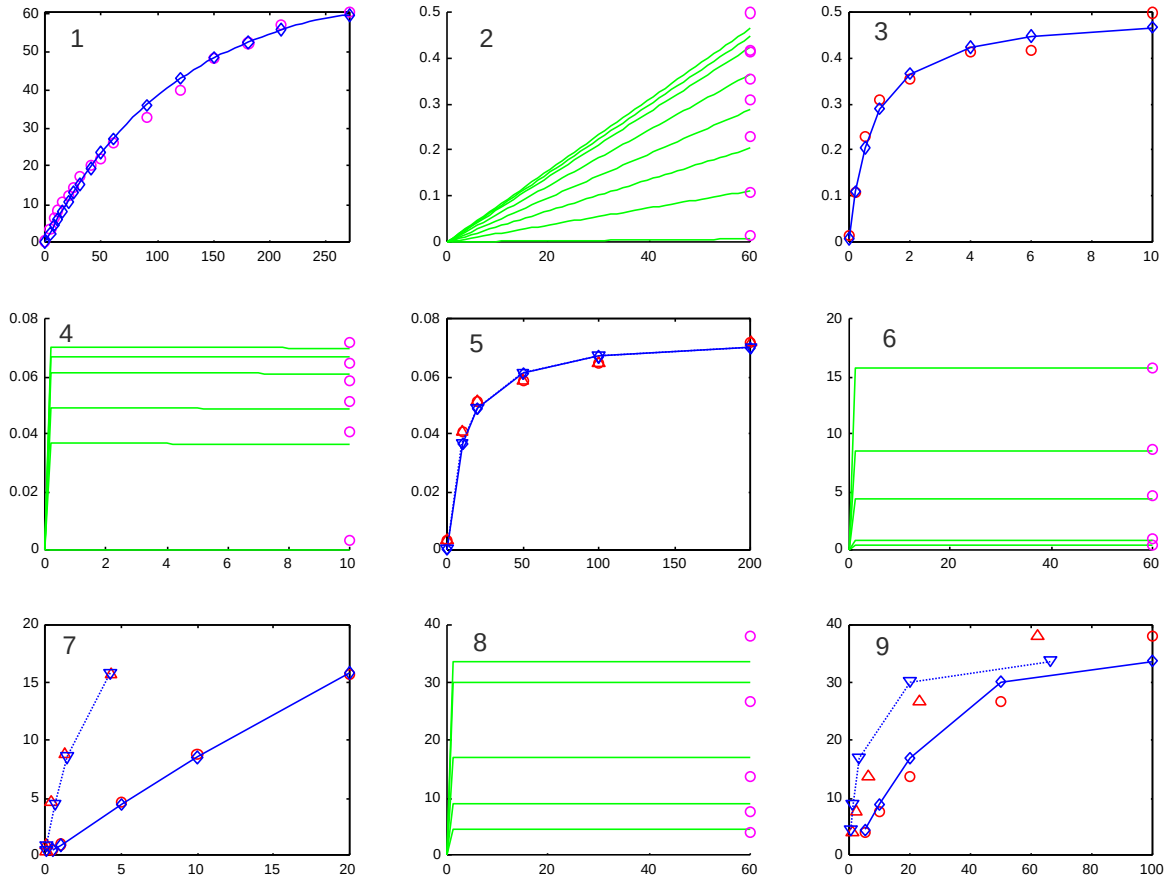

Figure S12. Kinetic model: data and model output

Data (red and magenta symbols) and model output (blue symbols and blue or green lines). The x-axes indicate time (min) or concentrations (µM) as indicated for the different panels below. The y-axes indicate concentrations (µM). The red circles in panels 5, 7 and 9 show the measured concentrations of adsorbed EDTA, Fe(II) and Fe(III)EDTA as a function of added concentrations, the red triangles as a function of measured dissolved concentrations in equilibrium. The blue diamonds show the modeled adsorbed equilibrium concentrations as function of added concentrations, the blue triangles as a function of the calculated dissolved equilibrium concentrations.

1 Batch dissolution experiment: [Fe(III)EDTA] vs. time after addition of Fe(II). $[Lp]_0$ = 1.13 mM.
2 FTIR dissolution experiments with added FeII: $[Fe(III)EDTA]_{diss.}$ vs. time. $[Lp]_0$ = 10 µM.
3 FTIR dissolution experiments with added FeII: $[Fe(III)EDTA]_{diss.}$ at t=3600 vs. added [Fe(II)]. $[Fe(III)[EDTA]_{diss}$ was calculated from dissolution rates measured by FTIR. $[Lp]_0$ =10 µM.
4 $[EDTA]_{ads}$ vs. time for fast equilibrium. $[Lp]_0$ = 10 µM.
5 $[EDTA]_{ads}$ vs. added and equilibrium conc. of $[EDTA]_{diss.}$ $[Lp]_0$ = 10 µM.
6 $[Fe(II)]_{ads}$ vs. time for fast equilibrium. $[Lp]_0$ = 28.1 mM.
7 $[Fe(II)]_{ads}$ vs. added and equilibrium conc. of $[EDTA]_{diss.}$ $[Lp]_0$ = 28.1 mM.
8 $[Fe(III)EDTA]_{ads}$ vs. time for fast equilibrium.
9 $[Fe(III)EDTA]_{ads}$ vs. added and equilibrium conc. of $[Fe(III)EDTA]_{diss.}$ $[Lp]_0$ = 28.1 mM.

Adsorption isotherms for Fe(II) and Fe(III)EDTA were measured in batch experiments with 2.5 g Lp/L (10 mM NaCl, 5 mM MES pH 6.0), reaction time 30 min. Fe-concentrations were measured with ICP-MS (Agilent 7500ce).[12]

Text S8. References

1. Borer, P. M.; Sulzberger, B.; Reichard, P.; Kraemer, S. M., Effect of siderophores on the light-induced dissolution of colloidal iron(III) (hydr)oxides. *Marine Chemistry* **2005,** *93*, 179– 193.
2. Borer, P.; Kraemer, S. M.; Sulzberger, B.; Hug, S. J.; Kretzschmar, R., Photodissolution of lepidocrocite (γ-FeOOH) in the presence of desferrioxamine B and aerobactin. *Geochimica et Cosmochimica Acta* **2009,** *73*, (16), 4673-4687.
3. Borer, P.; Sulzberger, B.; Hug, S. J.; Kraemer, S. M.; Kretzschmar, R., Wavelength-dependence of photoreductive dissolution of lepidocrocite (γ-FeOOH) in the absence and presence of the siderophore DFOB. *Environmental Science and Technology* **2009,** *43*, (6), 1871-1876.
4. Borer, P.; Sulzberger, B.; Hug, S. J.; Kraemer, S. M.; Kretzschmar, R., Photoreductive dissolution of iron(III) (Hydr)oxides in the absence and presence of organic ligands: Experimental studies and kinetic modeling. *Environmental Science and Technology* **2009,** *43*, (6), 1864-1870.
5. Schwertmann, U.; Cornell, R. M., *Iron Oxides in the Laboratory*. 2nd, Completely Revised and Extended Edition ed.; Wiley-VCH Weinheim, Germany, 2000.
6. Karametaxas, G.; Hug, S. J.; Sulzberger, B., Photodegradation of EDTA in the Presence of Lepidocrocite. *Environmental Science and Technology* **1995,** *29*, (12), 2992-3000.
7. Nowack, B.; Lutzenkirchen, J.; Behra, P.; Sigg, L., Modeling the adsorption of metal-EDTA complexes onto oxides. *Environmental Science & Technology* **1996,** *30*, (7), 2397-2405.
8. Nowack, B.; Sigg, L., Adsorption of EDTA and metal-EDTA complexes onto goethite. *Journal of Colloid and Interface Science* **1996,** *177*, (1), 106-121.
9. Samson, S. D.; Eggleston, C. M., The depletion and regeneration of dissolution-active sites at the mineral-water interface: II. Regeneration of active sites on alpha-Fe2O3 at pH 3 and pH 6. *Geochimica Et Cosmochimica Acta* **2000,** *64*, (21), 3675-3683.
10. Wehrli, B., Monte Carlo simulations of surface morphologies during mineral dissolution. *Journal of Colloid and Interface Science* **1989,** *132*, (1), 230-242.
11. Bhandari, N.; Hausner, D. B.; Kubicki, J. D.; Strongin, D. R., Photodissolution of Ferrihydrite in the Presence of Oxalic Acid: An In Situ ATR-FTIR/DFT Study. *Langmuir* **2010,** *26*, (21), 16246-16253.
12. Kang, K.; Schenkeveld, W. D. C.; Biswakarma, J.; Borowski, S. C.; Hug, S. J.; Hering, J. G.; Kraemer, S. M., The catalytic role of low Fe(II) concentrations in ligand-controlled dissolution of Fe(III) (hydr)oxide minerals. Environ. Sci. Technol. 2018. **DOI:** 10.1021/acs.est.8b03909.